Robotics & Computer-Integrated Manufacturing, Vol. 10, No. 4, pp. 301–309, 1993
Printed in Great Britain.

0736-5845/93 $6.00 + 0.00

● *Paper*

MAXIMUM ALLOWABLE LOAD OF FLEXIBLE MANIPULATORS FOR GIVEN DYNAMIC TRAJECTORY

Y. L. YAO,* M. H. KORAYEM† and A. BASU†

*School of Mechanical and Manufacturing Engineering, University of New South Wales, Kensington, NSW, 2033, Australia and †Department of Mechanical Engineering, University of Wollongong, Wollongong, NSW, 2522, Australia

This paper presents the formulation and numerical solution of the dynamic load carrying capacity (DLCC) problem of flexible manipulators. For manipulators under the rigid body assumption, the major limiting factor in determining the maximum allowable load (load mass and load moment of inertia) for a prescribed dynamic trajectory (positions, velocities and accelerations) is the joint actuator capacity. But for a flexible robot, an additional constraint on allowable deformation at the end effector must be imposed because either lighter-weight links or operating at a higher speed could cause unacceptable fluctuations when moving along a trajectory. A Lagrangian assumed mode method was used to model the manipulator and load dynamics, including both joint and deflection motions. The deflection equations are then coupled with robot kinematics to solve for the generalized coordinates. A strategy to determine the DLCC subject to both constraints mentioned above is formulated where the end effector deflection constraint is specified in terms of a series of spherical bounds with a radius equal to the allowable deformation. A general computational procedure for the multiple-link case given arbitrary trajectories is described in detail. Symbolic derivation and simulation by using a PC-based symbolic language MATHEMATICA® was carried out for a two-link planer robot. The results confirmed the necessity of the dual constraints and showed that which constraint is more critical for a given robot and trajectory depends on the required tracking accuracy.

NOMENCLATURE

- $\mathbf{A}_i$ joint transformation relates system i to system i-1
- $\mathbf{B}_f$ position and orientation of the end effector (for deformable links)
- $\mathbf{B}_r$ position and orientation of the end effector (for rigid links)
- c_a load coefficient due to actuator constraint
- c_{pr} load coefficient due to positional and rotational deformation constraints
- c_p load coefficient in terms of positional deformation constraint
- c_r load coefficient in terms of rotational deformation constraint
- $\mathbf{Def}_e$ end point deflection with end effector mass
- $\mathbf{Def}_n$ end point deflection without end effector mass
- $\mathbf{Def}_P$ positional deformation of the end effector
- $\mathbf{Def}_R$ orientational deformation of the end effector
- $\mathbf{g}$ gravity vector expressed at the base coordinate frame
- $\mathbf{h}_i$ position of a point on link i with respect to the base coordinates
- ${}^i\mathbf{h}_i$ vector from a point fixed in link i with respect to $Oixyz$
- $\mathbf{J}$ inertia matrix $\left(=\begin{bmatrix}[J_{jh}] & [J_{jhk}]\\ [J_{hjk}] & [I_{jfhk}]\end{bmatrix}\right)$
- $\mathbf{J}_r$ Jacobian matrix of rigid body manipulators
- $\mathbf{J}_f$ Jacobian matrix of flexible manipulators
- J_0, J_i actuator inertia at base joint and joint i
- K total kinetic energy of the robot/load system
- l_i length of link i
- m_e, I_e mass and moment of inertial of end effector (planer case)
- M_i mass concentrated at joint i
- m_i number of modes used to describe the deflection of link i
- n number of links
- q_h joint variable of the hth joint
- q_{hk} deflection variable (amplitude) of the kth model of link h
- $\mathbf{q}_r$ vectors of generalized coordinates for rigid body manipulators
- $\mathbf{q}_f$ vectors of generalized coordinates for flexible manipulators
- $\mathbf{R}$ vector of remaining dynamics and external forcing terms $(=[R_1, R_2 \ldots, R_h \ldots, R_n, R_{11}, R_{12}, \ldots, R_{1m_1}, R_{21} \ldots, R_{2m_2} \ldots, R_{h1} \ldots, R_{hm_n} \ldots, R_{nm_n}]^T$
- $\mathbf{r}_i$ vector locating the centre of mass of link i
- R_j dynamics from the joint equation j, excluding second derivatives of the generalized coordinates
- R_{jf} dynamics from the deflection equation jf, excluding second derivatives of the generalized coordinates
- R_P allowable deflection bound for a desired trajectory
- y_i deflection of link i at l_i
- $\mathbf{W}_i$ transformation from the base to the ith link
- $\mathbf{W}_{nr}$ equal to $\mathbf{W}_n$, when deformation is equal to zero
- V total potential energy of the robot/load system
- $\mathbf{z}$ vector of generalized coordinates $([q_1, q_2 \ldots, q_h \ldots, q_n, q_{11}, q_{12} \ldots, q_{1m_1}, q_{21} \ldots, q_{2m_2} \ldots, q_{h1} \ldots, q_{hm_n} \ldots, q_{nm_n}]^T)$
- μ_i spatial variable along link i
- ϕ_i rotational deformation of link i at l_i

INTRODUCTION

The load carrying capacity of a robot manipulator is often defined as the maximum payload that the manipulator can repeatedly lift in its fully extended configuration. But to determine the *dynamic* load carrying capacity (DLCC) of a robot must take into consideration the inertia effect of the load along a desired trajectory (positions, velocities and accelerations) as well as the manipulator dynamics. It has

been shown that, if the rigid body assumption is used, the DLCC of a manipulator is primarily constrained by the joint actuator torque characteristics.[10,11] Wang and Ravani[11] presented a method based on superposition of the dynamics of the load and the manipulator, where typical speed–torque characteristics for DC motors were assumed and an allowable load is calculated for each of the m points digitized along the trajectory. The maximum load is then the minimum value of these allowable loads. The robot will be able to carry an object and move along the trajectory as long as its mass and moment of inertia are not greater than the "maximum load" for that trajectory. Thomas *et al.*[10] have used the concept of DLCC as a design criteria for sizing the actuators for robot manipulators.

With the ever increasing demands on higher productivities, using existing robots at higher speeds and designing robots with lighter weights have been recognized as viable solutions. However, in either case the assumption of rigidity is challenged. Inevitable link deflections and oscillations at a higher speed undermine the theoretical foundation of the rigid body kinematics and dynamics. The limitations of the rigid link assumption in the formulation and analysis of flexible manipulator dynamics were investigated extensively, resulting in a number of formulations.[1–4,9] Recursive or non-recursive Lagrangian assumed mode,[2–4] generalized Newton–Euler,[9] and Lagrangian using Rayleigh–Ritz[1] methods are examples. As noted by Rakhsha and Goldenberg,[8] the effect of flexibility appears as an internal disturbance torque acting on the rigid body motion of the sytem, as seen from the dynamic equations of a flexible robot.

If one removes the rigid body assumption, the DLCC determined under the actuator constraint alone[11] will normally be too large. Because the DLCC so determined is adequate for the size of actuators, but does not guarantee how precisely the robot can track the given trajectory under such a load, the resultant end effector deflection or oscillation at a higher speed may prove too large to accept for applications requiring precision tracking. Therefore, an additional constraint must be imposed when the DLCC is to be determined for flexible manipulators. The constraint should account for the main difference between rigid and flexible manipulators.

This paper presents a new method to determine the DLCC for flexible manipulators, subject to *both* actuator *and* end effector deflection constraints. First, the recursive Lagrangian assumed mode method[2] was modified to accommodate the load dynamics, which together with kinematic equations are necessary to determine the DLCC. A strategy of determining the DLCC subject to both constraints is then described, where a series of spherical bounds centred at the desired trajectory is used in the end effector oscillation constraint while a typical DC motor speed–torque characteristics curve is used in the actuator constraint. The dependence of both the magnitude and frequency characteristics of the end effector oscillation on load is accounted for. A general computational procedure is presented for the DLCC of multiple-link manipulators for any given dynamic trajectory. Finally, a numerical example involving a two-link flexible manipulator using the method is presented and the results are discussed.

LAGRANGIAN ASSUMED MODE MODELLING INCORPORATING LOAD DYNAMICS

To determine the DLCC for flexible manipulators, proper modelling of manipulator and load dynamics is a prerequisite. The method employed here largely follows that of Ref. 2, except that the dynamic effects of load at the end effector as well as the mass at joints to account for actuatory and gearing inertia were added. The deformation of the robot links is assumed to be a general one about the link neutral axis, denoted by $x=\mu$. It is assumed that end effector deflection is primarily caused by link deflection or oscillation at higher speeds, and links are slender beams. After its kinematics is set up, the kinetic energy K and potential energy V of the manipulator and load system can be expressed as follows:

$$K=\sum_{i=1}^{n}\frac{1}{2}\int_0^{l_i}\mathrm{Tr}\,\{\dot{\mathbf{h}}_i\dot{\mathbf{h}}_i^T\}\,\mathrm{d}m + \frac{1}{2}J_0\,\mathrm{Tr}\left\{\left(\frac{\partial^1\dot{\mathbf{h}}_1}{\partial\mu_1}\right)\left(\frac{\partial^1\dot{\mathbf{h}}_1^T}{\partial\mu_1}\right)_{(\mu_1=0)}\right\} + \sum_{i=1}^{n}\mathrm{Tr}\left[\frac{1}{2}J_i\left(\frac{\partial^i\dot{\mathbf{h}}_i}{\partial\mu_i}\right)\left(\frac{\partial^i\dot{\mathbf{h}}_i^T}{\partial\mu_i}\right)_{(\mu_i=l_i)} + \frac{1}{2}M_i\{\dot{\mathbf{h}}_i\dot{\mathbf{h}}_i^T\}_{(\mu_i=l_i)}\right] \tag{1}$$

$$V=-\sum_{i=1}^{n}\mathbf{g}^T\mathbf{W}_i\mathbf{r}_i+\sum_{i=1}^{n}\sum_{k=1}^{m_i}\sum_{l=1}^{m_i}q_{ik}q_{il}K_{ikl} \tag{2}$$

where the first term of the kinetic energy is identical to Ref. 2 while the rest of the terms are different in order to account for the load effect M_n and joint mass effect M_i, for $i=1$ to $n-1$. By using Lagrange's equations of motion, the dynamic equations of a flexible manipulator are obtained with generalized coordinates q_h and q_{hk}. The resultant system of equations can be organized in matrix form as

$$\sum_{h=1}^{n}J_{jh}\ddot{q}_h+\sum_{h=1}^{n}\sum_{k=1}^{m_h}J_{jhk}\ddot{q}_{hk}=R_j \tag{3}$$

for joint j and

$$\sum_{h=1}^{n}J_{jhf}\ddot{q}_h+\sum_{h=1}^{n}\sum_{k=1}^{m_h}I_{jfhk}\ddot{q}_{hk}=R_{jf} \tag{4}$$

for mode f of link j, or, in a combined matrix form,

$$\mathbf{J}\ddot{\mathbf{z}}=\mathbf{R} \tag{5}$$

where the elements of **J** and **R** are slightly different from that given in Ref. 2. For instance, the coefficients $\mathbf{C}_i$, $\mathbf{C}_{ij}$ and $\mathbf{C}_{ijk}$ take the form

$$\mathbf{C}_i = 1/2 \int_0^{l_i} [1, \mu_i, 0, 0]^T [1, \mu_i, 0, 0]\, dm + 1/2 M_i [1, \mu_i, 0, 0]^T [1, \mu_i, 0, 0]_{(\mu_i = l_i)} \quad (6a)$$

$$\mathbf{C}_{ij} = 1/2 \int_0^{l_i} [1, \mu_i, 0, 0]^T [0, x_{ij}, y_{ij}, z_{ij}]\, dm + 1/2 M_i [1, \mu_i, 0, 0]^T [0, x_{ij}, y_{ij}, z_{ij}]_{(\mu_i = l_i)} \quad (6b)$$

$$\mathbf{C}_{ijk} = 1/2 \int_0^{l_i} [0, x_{ij}, y_{ij}, z_{ij}]^T [0, x_{ij}, y_{ij}, z_{ij}]\, dm + 1/2 M_i [0, x_{ij}, y_{ij}, z_{ij}]^T [0, x_{ij}, y_{ij}, z_{ij}]_{(\mu_i = l_i)} \quad (6c)$$

$$\mathbf{S}_{ijk} = 1/2 \left(\frac{\partial}{\partial \mu}\right) [0, x_{ij}, y_{ij}, z_{ij}]^T \left(\frac{\partial}{\partial \mu}\right) [0, x_{ij}, y_{ij}, z_{ij}]. \quad (6d)$$

Other minor differences are in the dynamic equation, where the coefficient I_{jfnk} becomes

$$I_{jfnk} = 2\ \mathrm{Tr}\{\mathbf{W}_j \mathbf{M}_{jf}^j \mathbf{W}_n \mathbf{D}_{nk} \mathbf{W}_h^T + J_j \mathbf{S}_{ijk}\} \quad (7)$$

and in the recursive equation where the recursive expression ${}^j\mathbf{F}_h$ should be ${}^j\mathbf{F}_h = {}^j\tilde{\mathbf{F}}_{h+1} \mathbf{A}_{h+1}^T$.

DLCC FOR A GIVEN TRAJECTORY

Given a trajectory (positions, velocities and accelerations), the DLCC of a flexible manipulator is defined as the maximum load (mass and moment of inertia) that the manipulator can carry in executing the trajectory with an acceptable tracking accuracy. The tracking accuracy is emphasized because we deal with flexible robots. In particular, this is dealt with by introducing a constraint on end effector deflection, in addition to the joint torque capacity constraint often imposed alone for rigid manipulators. This is necessary because deflection of the robot at its end effector can cause excessive deviations from the given trajectory, even though the joint torque constraint is not violated.

End effector deflection constraint

Deflection at the end effector could be attributed to both static and dynamic factors, such as link flexibility, joint clearance, manipulator and load inertia. These factors are configuration or motion-dependent; therefore, the DLCC varies from place to place on a given trajectory. A constraint should be imposed in such a way that the worst case, which corresponds to the least DLCC, is used to determine the maximum load.

A given trajectory is first digitized into m points. No load defection, $(\mathbf{Def}_n)_j$, and defection with added end effector mass, $(\mathbf{Def}_e)_j$, are calculated for $j = 1, 2, \ldots, m$, using the computational procedure outlined in the next section. As seen in Fig. 1, the additional mass at the end effector changes both the magnitude and the direction of the deflection. But as long as the magnitude of the deflection is less than or equal to an allowable value, the robot is considered to be still capable of executing the given trajectory. In other words, only the magnitude of the deflections $(\mathrm{Def}_n)_j$ and $(\mathrm{Def}_e)_j$ need be of concern in this context. This prompted the use of a spherical boundary of radius R_p as the end effector deflection constraint and the sphere is centred at the desired position on the given trajectory. Although $(\mathbf{Def}_n)_j$ and $(\mathbf{Def}_e)_j$ are generally vectors of different directions, the magnitude increase due to the added mass at the end effector is linearly related to the mass.[5] Therefore, the difference between the allowable deflection and the magnitude of the defection with added end effector mass at point j

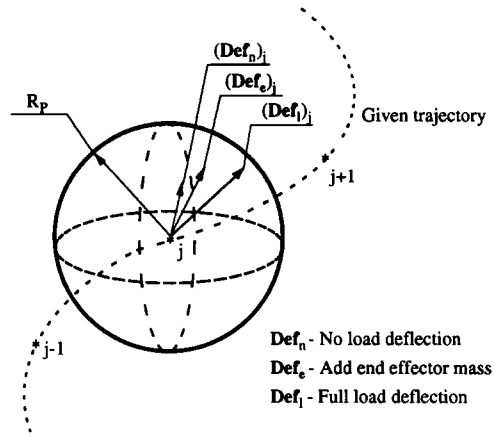

Fig. 1. Spherical boundary of end effector deflections.

$$R_p - (\mathrm{Def}_e)_j \quad (8)$$

can be regarded as the remaining amount of end effector deflector which can still be accommodated at point j of the given trajectory. It is this remaining amount that indicates how much load can be carried through the point j without violating the deflection constraint.

What further complicates the problem is the fact that a load not only affects the magnitude of deflection but also its frequency, which is evident from Figs 2 and 3. As seen in Fig. 2, for an arbitrary trajectory the full load case gives a larger deflection and lower fluctuating rate than the no-load case and the case with added end effector mass. This can be better observed from the hand coordinate system in Fig. 3. When the full load case exhibits about two and a half oscillations, the other cases exhibit about three and three and a half, respectively. Therefore, it is necessary to introduce the concept of a load coefficient $(c_p)_j$ for point j, $j = 1, 2, \ldots, m$, as follows:

$$(c_P)_j = \frac{R_p - (\mathrm{Def}_e)_j}{\max\{\mathrm{Def}_e\} - \max\{\mathrm{Def}_n\}} \quad (9a)$$

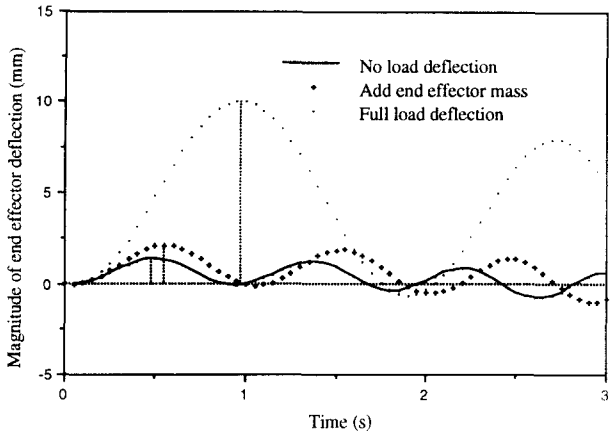

Fig. 2. Dependence of deflection magnitude and frequency on load.

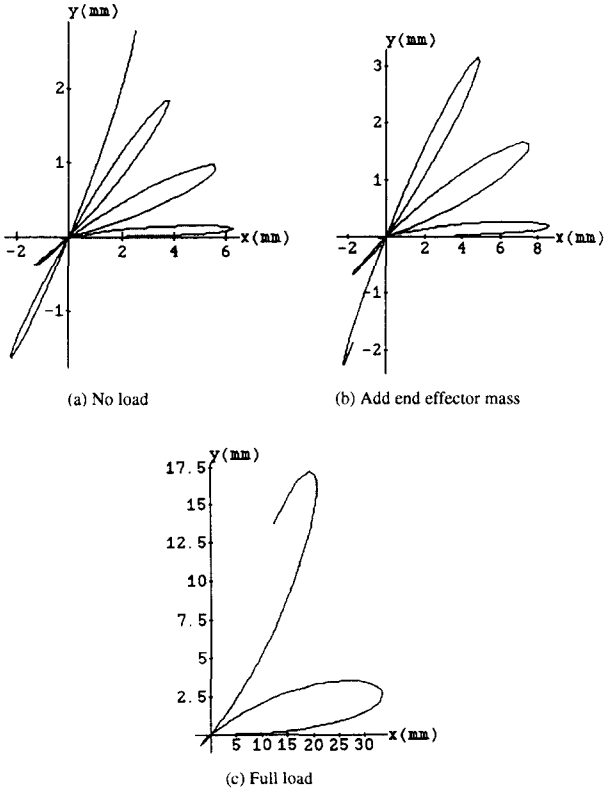

Fig. 3. Dependence of deflection magnitude and frequency on load viewed in hand coordinate system.

where

$$\max\{\mathrm{Def}_e\} = \max\{(\mathrm{Def}_e)_1, (\mathrm{Def}_e)_2, \ldots, (\mathrm{Def}_e)_m\} \quad (9b)$$

$$\max\{\mathrm{Def}_n\} = \max\{(\mathrm{Def}_n)_1, (\mathrm{Def}_n)_2, \ldots, (\mathrm{Def}_n)_m\}. \quad (9c)$$

The rotational deflections can be similarly represented in terms of vectors, and their magnitudes be compared to a spherical boundary of radius R_r specified in a hand coordinate system. A load coefficient for rotation $(c_r)_j$ similar to Eq. (8) can be defined for each point j, $j=1, 2, \ldots, m$. Finally, a load coefficient satisfying both positional and rotational deflection constraints is obtained as follows:

$$(c_{pr})_j = \min\{(c_p)_j, (c_r)_j\} \quad j=1, 2, \ldots, m. \quad (10)$$

Joint actuator torque constraint

The joint actuator torque constraint is formulated based on the typical torque–speed characteristics of DC motors as follows,[11] while other actuation systems can be dealt with similarly:

$$u_a^{(+)} = k_1 - k_2\dot{q} \quad (11a)$$

$$u_a^{(-)} = -k_1 - k_2\dot{q} \quad (11b)$$

where $k_1 = \tau_s$, $k_2 = \tau_s/w_0$, τ_s is the stall torque, w_0 is maximum no-load of the motor, and $u_a^{(+)}$ and $u_a^{(-)}$ are the upper and lower bounds of the allowable torque. Using the computational procedure outlined in the next section, the ith joint torque due to a n-link manipulator dynamics and the added end effector mass, $(\tau_e)_i$, $i=1, 2, \ldots, n$, can be computed for each point of the given trajectory. Together with the upper and lower bounds computed using Eqs (11a) and (11b), the upper and lower bounds on torques available for load can be expressed:

$$\tau_i^{(+)} = (u_a^{(+)})_i - (\tau_e)_i \quad (12a)$$

$$\tau_i^{(-)} = (u_a^{(-)})_i - (\tau_e)_i. \quad (12b)$$

The maximum allowable torque at joint i is then equal to

$$(\tau_a)_i = \max\{\tau_i^{(+)}, \tau_i^{(-)}\}. \quad (12c)$$

Equations (12a) and (12b) remain valid for flexible manipulators because the linearity between the force $\mathbf{F}$ acting on the end effector (a load can be modelled as an inertial force on the tip) and the corresponding joint torques τ is preserved if small deformations are assumed. This can be shown by using the virtual work principle. The virtual work done by $\mathbf{F}$ and τ is given by

$$\begin{aligned}\delta w &= \tau^T \delta\mathbf{q}_r + \tau^T \delta\mathbf{q}_f - \mathbf{F}^T \Delta\mathbf{p} \\ &= \tau^T \delta\mathbf{q}_r + \tau^T \delta\mathbf{q}_f - \mathbf{F}^T\mathbf{J}_r \delta\mathbf{q}_r \\ &\quad - \mathbf{F}^T\mathbf{J}_f \delta\mathbf{q}_f \end{aligned} \quad (13)$$

where $\delta\mathbf{q}_r$, and $\delta\mathbf{q}_f$ are the infinitesimal changes of the generalized coordinates corresponding to joint rotations and link deflections, respectively, $\mathbf{J}_r$ and $\mathbf{J}_f$ are the Jacobians corresponding to joint rotations and link deflections, respectively, and $\Delta\mathbf{p}$ is the infinitesimal translation and rotation at the end effector. With further simplifications, one can obtain

$$\delta w = [\tau^T - \mathbf{F}^T\mathbf{J}_r\tau^T - \mathbf{F}^T\mathbf{J}_f]\begin{bmatrix}\delta\mathbf{q}_r \\ \delta\mathbf{q}_f\end{bmatrix} = [\tau^T - \mathbf{F}^T\mathbf{J}_g][\delta\mathbf{q}_g] \quad (14)$$

where $\mathbf{J}_g = [\mathbf{J}_r\mathbf{J}_f]$, and $\mathbf{q}_g = [\mathbf{q}_r\mathbf{q}_f]$.

In order for Eq. (14) to vanish for arbitrary $\delta\mathbf{q}_g$, we must have

$$\tau = \mathbf{J}_g^T\mathbf{F}. \quad (15)$$

For the same reason given for Eq. (9), a load coefficient complying with the actuator torque constraint can be

calculated for each point j, $j=1, 2, \ldots, m$, of a given trajectory as follows:

$$(c_a)_j = \min\left\{\frac{(\tau_a)_i}{\max\{\tau_e\}-\max\{\tau_n\}},\quad i=1,\ldots,n\right\} \quad (16a)$$

where τ_n is the no-load torque and

$$\max\{\tau_e\} = \max\{(\tau_e)_1, (\tau_e)_2, \ldots, (\tau_e)_m\} \quad (16b)$$

$$\max\{\tau_n\} = \max\{(\tau_n)_1, (\tau_n)_2, \ldots, (\tau_n)_m\}. \quad (16c)$$

Determination of maximum load

To guarantee that both the end effector deflection and joint torque capacity constraints are satisfied at each of the m digitized points of a given trajectory, a load coefficient c can be found from $(c_{pr})_j$ and $(c_a)_j$, each of which is associated with a constraint, as follows:

$$c = \min\{(c_{pr})_j,\quad (c_a)_j,\quad j=1,\ldots,m\}. \quad (17a)$$

Then, the maximum mass for this trajectory is

$$m_{\text{load}} = cm_e \quad (17b)$$

and the maximum principle moment of inertia of the load is

$$[I_{\text{load}}] = c[I_e] \quad (17c)$$

where m_e and $[I_e]$ are end effector mass and moment of inertia, respectively. The maximum load is then specified by the values of both m_{load} and $[I_{\text{load}}]$. As long as the actual mass and moment of the inertia of the load are not greater than the "maximum load" for that trajectory, the actuators are adequate to execute the trajectory within the allowable end effector deflection.

COMPUTATIONAL PROCEDURE

The computational produce for determining the DLCC is outlined and also flow-charted in Fig. 4. The manipulator Jacobians associated with joint rotations and ink deflections, $\mathbf{J}_r$ and $\mathbf{J}_f$, are calculated first. The infinitesimal translation and rotation of the end effector, $d\mathbf{X}_e$ and $d\mathbf{\Phi}_e$, and their derivatives are expressed as

$$d\mathbf{p} = [d\mathbf{X}_e\ d\mathbf{\Phi}_e]^T \quad \text{and} \quad \dot{\mathbf{p}} = [\mathbf{V}_e\ \bar{\boldsymbol{\omega}}_e]^T. \quad (18)$$

On the other hand, $d\mathbf{p}$ can be written in terms of the differential changes in joint variables as well as the differential changes in displacements at the free end of the end link due to link deformations as

$$d\mathbf{p} = \mathbf{J}_r\, d\mathbf{q}_r + \mathbf{J}_f\, d\mathbf{q}_f \quad \text{and} \quad \dot{\mathbf{p}} = \mathbf{J}_r\dot{\mathbf{q}}_r + \mathbf{J}_f\dot{\mathbf{q}}_f. \quad (19)$$

By differentiating once more, one obtains

$$\ddot{\mathbf{p}} = \mathbf{J}_r\ddot{\mathbf{q}}_r + \mathbf{J}_f\ddot{\mathbf{q}}_f + \dot{\mathbf{J}}_r\dot{\mathbf{q}}_r + \dot{\mathbf{J}}_f\dot{\mathbf{q}}_f \quad (20a)$$

or

$$\mathbf{J}_r\ddot{\mathbf{q}}_r + \mathbf{J}_f\ddot{\mathbf{q}}_f = \ddot{\mathbf{p}} - \dot{\mathbf{J}}_r\dot{\mathbf{q}}_r - \dot{\mathbf{J}}_f\dot{\mathbf{q}}_f. \quad (20b)$$

The above kinematic expression is essential but not adequate for solving all the generalized coordinates by given $\mathbf{p}$, $\dot{\mathbf{p}}$ and $\ddot{\mathbf{p}}$. To obtain precise solutions for generalized coordinates, Eq. (21) must be solved simultaneously with the deflection equations [Eq. (4)], with and without end effector mass. The equations, however, are highly coupled and nonlinear. Furthermore, they are so lengthy that it is extremely difficult, if not impossible, to expand them manually even for a lower degree of freedom manipulator with a lower number of modes assumed. By using a symbolic derivation language, such as MATHEMATICA® described in the next section, symbolic derivation and deductions can be carried out automatically before the equations are numerically solved such that relatively insignificant terms such as second-order deformations may be examined and subsequently neglected with relative ease.

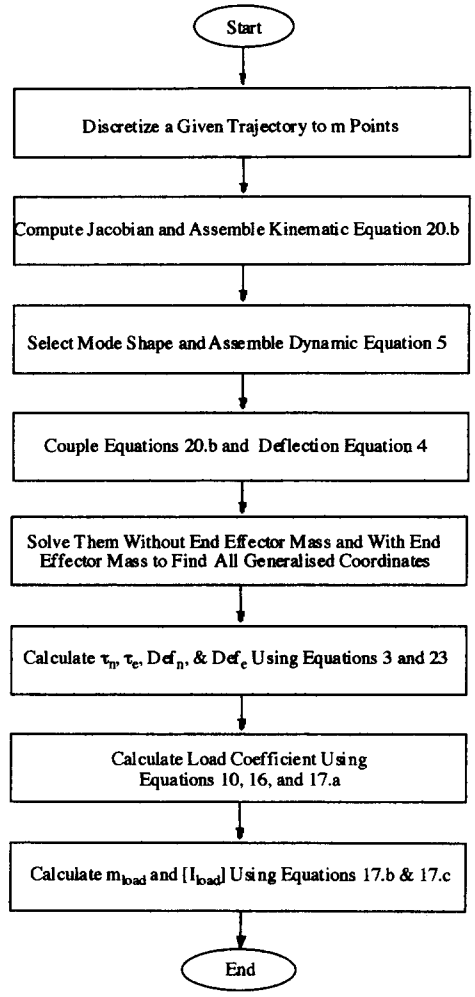

Fig. 4. Computational procedure.

After all the generalized coordinates are determined by numerically solving the nonlinear and coupled system of equations represented by Eqs (4) and (2) simultaneously, the next step is to compute rotational and translational deflections at the end effector, which are needed in determining the load coefficients associated with the end effector deflection constraint $(c_{pr})_j$ for $j=1,2,\ldots,m$ [Eq. (10)]. The position and orientation of the end effector assuming flexible links are given as

$$\mathbf{B}_f = \mathbf{W}_n\mathbf{A}_{n+1} \quad (21)$$

while for rigid links the end effector position and rotation are given as follows:

$$\mathbf{B}_r = \mathbf{W}_{nr}\mathbf{A}_{n+1} \tag{22}$$

such that deformation at the end effector is

$$\mathbf{Def} = \mathbf{B}_f - \mathbf{B}_r = (\mathbf{W}_n - \mathbf{W}_{nr})\mathbf{A}_{n+1} \tag{23}$$

and the elements of the **Def** matrix can be shown as

$$\mathbf{Def} = \begin{bmatrix} 1 & \mathbf{0}^T \\ \mathbf{Def}_p & \mathbf{Def}_R \end{bmatrix}. \tag{24}$$

In order to calculate the load coefficients associated with the joint capacity constraint $(c_a)_j$ for $j = 1, 2, \ldots, m$ [Eq. (16)], joint equations [Eq. (3)] are used to obtain τ_n and τ_e, given all the generalized coordinates calculated above. Finally, a load coefficient satisfying both constraints c is calculated [Eq. (17a)] and the maximum load for the given trajectory is determined in terms of m_{load} and $[I_{\text{load}}]$ by using Eqs (17b) and (17c). The procedure outlined here is applicable to any number of degree of freedom manipulator, any number of deflection modes assumed, and arbitrary trajectories.

SIMULATION RESULTS AND DISCUSSIONS

Simulation conditions

A simulation study was carried out to further investigate the validity and effectiveness of the method and computational procedure presented above. Computing the DLCC of a given trajectory is presented for a two-link flexible manipulator shown in Fig. 5. Only link flexibilities are considered while joint compliances are neglected. The bending deflections of links are approximated with simply supported mode shape for each link. Mode shapes are chosen from analytical solution of a Euler–Bernoulli beam eigenfunction analysis. Gravity effect was ignored in this case study in order to isolate the dynamic flexibility effects. The following system of equations can be assembled

(i) Kinematic equations

$$J_{r11}\ddot{q}_1 + J_{r12}\ddot{q}_2 + J_{f11}\ddot{q}_{11} + J_{f12}\ddot{q}_{21} = R_{t1} \tag{25a}$$

$$J_{r21}\ddot{q}_1 + J_{r22}\ddot{q}_2 + J_{f11}\ddot{q}_{11} + J_{f12}\ddot{q}_{21} = R_{t2} \tag{25b}$$

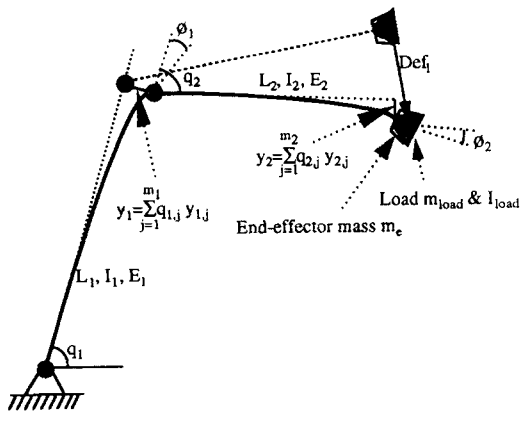

Fig. 5. Two-link flexible manipulator model.

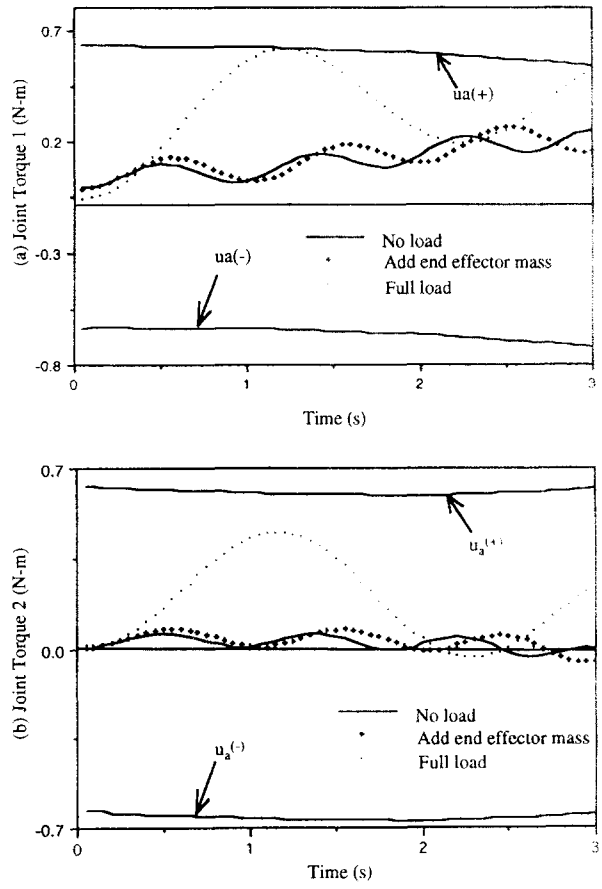

Fig. 6. Joint torques against torque bounds ($m_{\text{load}} = 0.5$ kg, subject to actuator torque constraint only).

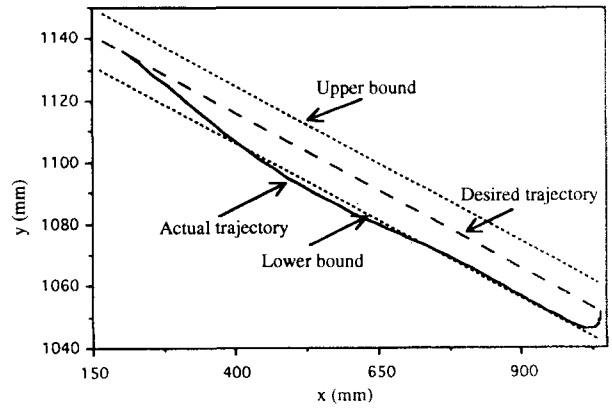

Fig. 7. Desired and actual trajectories against deflection bounds ($m_{\text{load}} = 0.5$ kg, under actuator constraint only).

where the expression of rigid body Jacobian $\mathbf{J}_r$ and flexible Jacobian $\mathbf{J}_f$ are given in Appendix 1.

(ii) Dynamic equations based on Lagrangian assumed mode method:

(a) Joint equations

$$J_{11}\ddot{q}_1 + J_{12}\ddot{q}_2 + J_{111}\ddot{q}_{11} + J_{121}\ddot{q}_{21} = R_1 \tag{26a}$$

$$J_{21}\ddot{q}_1 + J_{22}\ddot{q}_2 + J_{211}\ddot{q}_{11} + J_{212}\ddot{q}_{21} = R_2. \tag{26b}$$

(b) Deflection equations

$$I_{111}\ddot{q}_1 + I_{112}\ddot{q}_2 + I_{1111}\ddot{q}_{11} + I_{1121}\ddot{q}_{21} = R_{11} \tag{27a}$$

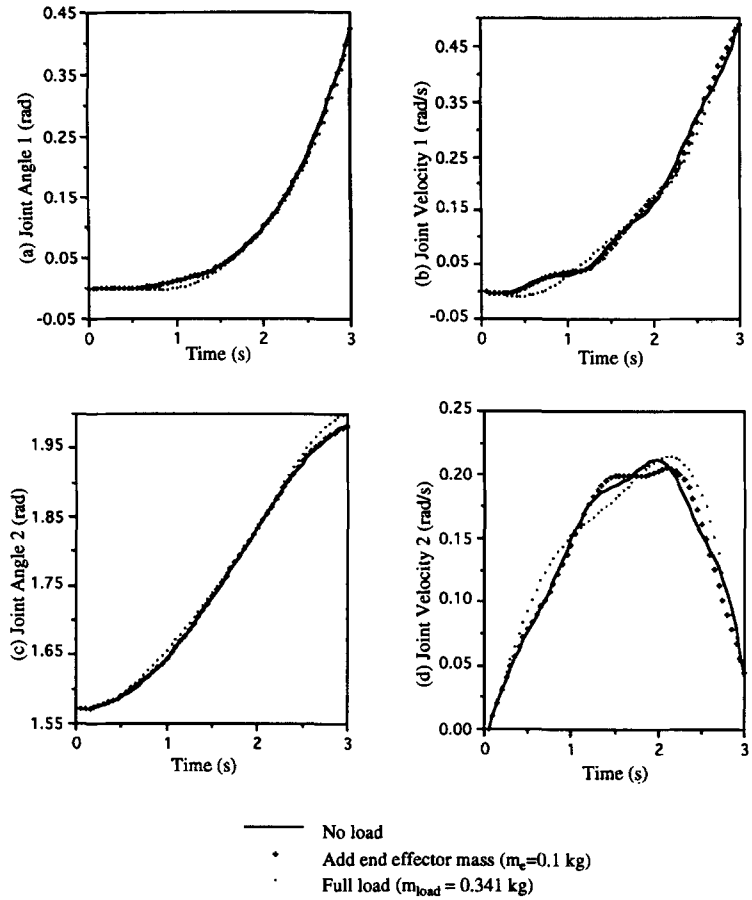

Fig. 8. Comparison of joint responses (under both constraints).

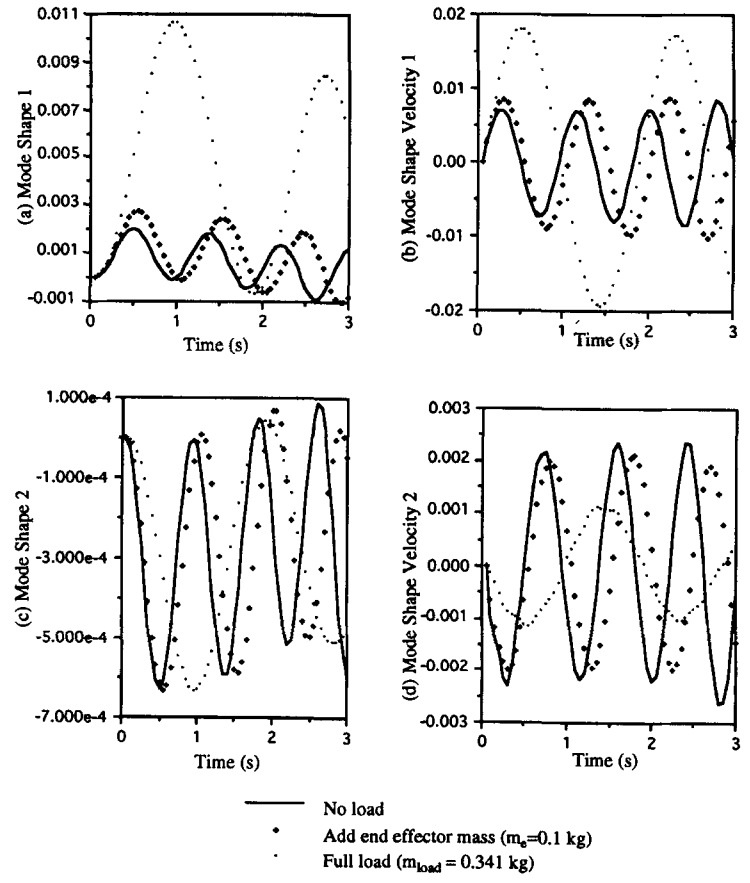

Fig. 9. Comparison of the mode shapes (under both constraints).

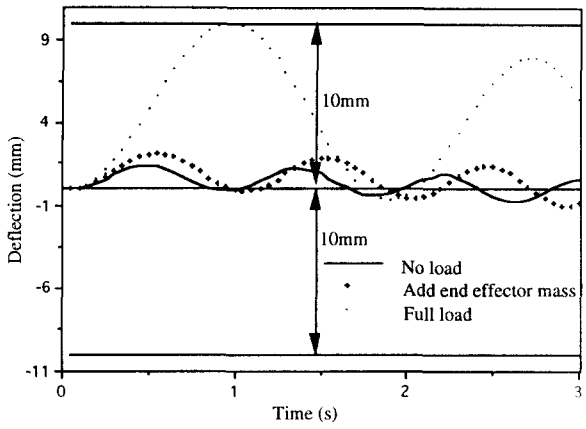

Fig. 10. Deflection against its bounds ($m_{load}=0.341$ kg, under both constraints).

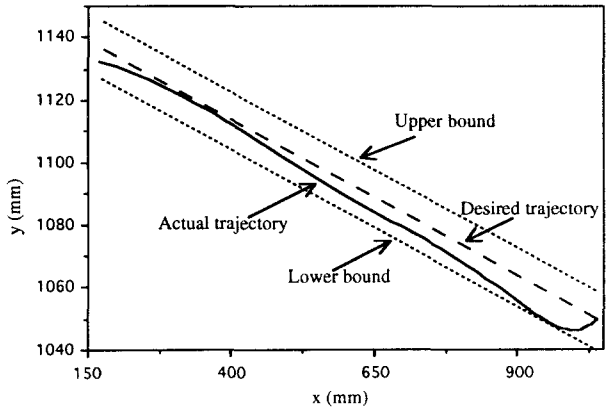

Fig. 11. Desired and actual trajectory ($m_{load}=0.341$ kg, under both constraints).

$$I_{211}\ddot{q}_1+I_{212}\ddot{q}_2+I_{2111}\ddot{q}_{11}+I_{2121}\ddot{q}_{21}=R_{21}. \quad (27b)$$

The numerical values used in the simulation are listed in the Appendix 2.

Symbolic derivation language

The much greater complexity of flexible manipulator dynamics literally forbids any practical manual symbolic derivations. Therefore, the advantages promised by symbolic manipulation programs are even desirable for flexible manipulators. The symbolic derivation of flexible manipulator dynamics was reported by Cetinkunt and Book[3,4] who have written a symbolic manipulation program based on SMP and simulated with a VAX-11/750 minicomputer.

This work used MATHEMATICA® for symbolic derivation, numerical solution, as well as DLCC determination.[6,7] It was chosen mainly because of its versatile symbolic manipulation capabilities, such as symbolic simplification of polynomials and rational expressions, linearization of trigonometric functions, automated evaluation of the relative significance of terms and subsequently, neglecting the less significant terms, and symbolic integration and differentiation.[12] It has an integrated graphics environment and can communicate at a high level with other programs using the MathLink communication standard.

Results and discussion

Various desired trajectories were simulated and a simple one is prescribed in its parametric form as follows:

$$x_d(t)=L-at^2, \quad \text{and} \quad y_d(t)=L+bt^2 \quad (28)$$

where L is the link length of both links, $a=0.1$, $b=0.01$, and t ranges from 0 to 3 sec. Velocities and accelerations are obtained by differentiating the trajectory. The initial conditions for all the generalized coordinates were taken to be zero except that $q_2(0)$ equals to 90°. The relative simplicity is meant to expose the features of the method without loss of generality. The trajectory was digitized to 64 points.

First, only the joint actuator torque constraint was imposed in determining the DLCC and a load $m_{load}=0.5$ kg was found to be the maximum load that the given actuators can carry in executing the trajectory, while the load moment of inertia I_{load} was not presented for simplicity. Figure 6 shows the time-varying torques required to execute the trajectory against the upper and lower bounds of the available torques which depend on the joint velocities. It is seen that the load so determined uses joint 1 to its maximum extent at about 1.2 sec while joint 2's bounds are not reached during the course. This indicates that the load determined by using the method is based on the "weakest" joint actuator, as it should be. However, when the actual trajectory is plotted in terms of the base coordinates with the prescribed upper and lower bounds $R_p=10$ mm in Fig. 7, it is apparent that the desired tracking accuracy cannot be achieved with $m_{load}=0.5$ kg because part of the actual trajectory is outside of the lower bounds. This clearly demonstrates the need to impose an additional constraint on end effector deflections when the DLCC is determined for flexible manipulators.

Both constraints were then imposed in determining the DLCC for the same robot, trajectory, and end effector deflection requirements. Again only the mass portion of the DLCC was calculated for simplicity. A load $m_{load}=0.341$ kg was found to be the maximum load that can be carried in executing the trajectory while not violating either of the constraints. The dotted lines in Fig. 8 denote the changes in joint angles and their rate when this load is carried to execute the trajectory, while these in Fig. 9 denote the changes in link mode shapes and their rate. Shown in Fig. 10 is the magnitude of the end effector deflection with such a load compared to the imposed upper and lower bounds. It is seen that all the magnitudes remain within the bounds because the load was determined subject to both constraints. The actual trajectory is further plotted in terms of the base coordinates in Fig. 11, which again shows it is within the bounds.

CONCLUSIONS

The main objective of this investigation is to formulate the DLCC and to determine the "maximum load" for flexible manipulators given a dynamic trajectory. This

was achieved by subjecting the manipulator to dual constraints, that is, actuator capacity and end effector deformation constraints, when the maximum load is determined. Simulation results show that, if only the first constraint is imposed for flexible manipulators as for rigid body manipulators, the load so determined may result in substantial deflections at the end effector when it moves through the prescribed dynamic trajectory. In order to be able to control the end effector tracking precision, adding the second constraint is necessary. Whether the first or second constraint is more strict depends on the required tracking accuracy. In the simulation results presented in this paper, the second one is more strict. This work also shows that dealing with flexible manipulator dynamics and determining their DLCC in particular greatly benefited from using a symbolic derivation language.

REFERENCES

1. Asada, H., Ma, Z.-D., Tokumaru, H.: Inverse dynamics of flexible robot arms: modeling and computation for trajectory control. *Trans. ASME J. dyn. Systems Meas. Control* **112**: 177–185, 1990.
2. Book, W. J.: Recursive lagrangian dynamics of flexible manipulator arm. *Int. J. Robotics Res.* **3**(3): 87–101, 1984.
3. Cetinkunt, S., Book, W. J.: Symbol modelling and dynamic simulation of the robotic manipulators with compliant links and joints. *Robotics* **5**(4): 301–310, 1989.
4. Cetinkunt, S., Book, W. J.: Symbolic modelling of flexible manipulators. In *Proceedings of* 1987 *IEEE International Conference on Robotics and Automation*, Raleigh, NC, 31 March–3 April 1987, Vol. 3, pp. 2074–2080.
5. Chen, J. S., Menq, C. H.: Experiments on the payload-adaptation of a flexible one-link manipulator with unknown payload. In *Proceedings of IEEE International Conference on Robotics and Automation*. 1990, pp. 1614–1619.
6. Korayem, M. H., Yao, Y., Basu, A.: Load carrying capacity for a two-link planer-flexible arm. In *Proceedings of Thirteenth Canadian Congress of Applied Mechanics*. 1991, Vol. 2, pp. 664–665.
7. Korayem, M. H., Yao, Y., Basu, A.: Symbolic derivation and dynamic simulation of flexible manipulators. In *Proceedings of International Conference on Intelligent Control and Instrumentation*, 18–21 February 1992.
8. Rakhsha, F., Goldenberg, A. A.: Dynamics modelling of a single-link flexible robot. In *Proceedings of International IEEE Conference on Robotics and Automation*. 1985, pp. 984–989.
9. Shabana, A. A.: Dynamics of flexible bodies using generalized Newton–Euler equation. *Trans. ASME J. dyn. Systems Meas. Control* **112**: 496–503, 1990.
10. Thomas, M., Yuan-Chou, H. C., Tesar, D.: Optimal actuator sizing for robotic manipulators based on local dynamic criteria. *ASME J. Mech. Transn Automn Design* **107**: 163–169, 1985.
11. Wang, L. T., Ravani, B.: Dynamics load carrying capacity of mechanical manipulators—Part I: problem formulation. *Trans ASME J. dyn. Systems Meas. Control* **110**: 46–52, 1988.
12. Wolfram, S.: *MATHEMATICA*. Reading, MA, Addison–Wesley. 1991.

APPENDIX 1: THE EXPRESSION OF RIGID BODY JACOBIAN J_r AND FLEXIBLE JACOBIAN J_F FOR SIMULATION

$$
\begin{aligned}
J_{r11} &= -l_1 \sin(q_1) - y_1 \cos(q_1) - (l_2 - y_2\phi_1) \\
&\quad \sin(q_1+q_2) - (l_2\phi_1 + y_2)\cos(q_1+q^2) \\
J_{r12} &= -(l_2 - y_2\phi_1)\sin(q_1+q_2) - (l_2\phi_1 + y_2)\cos(q_1+q_2) \\
J_{r21} &= -l_1\cos(q_1) - y_1 \sin(q_1) - (l_2\phi_1 + y_2) \\
&\quad \sin(q_1+q_2) + (l_2 - y_2\phi_1)\cos(q_1+q_2) \\
J_{r22} &= -(l_2\phi_1 + y_2)\sin(q_1+q_2) + (l_2 - y_2\phi_1)\cos(q_1+q_2) \\
J_{f11} &= -\sin(q_1) \\
J_{f12} &= -\sin(q_1+q_2) - \phi_1 \cos(q_1+q_2) \\
J_{f21} &= \cos(q_1) \\
J_{f22} &= \cos(q_1+q_2) - \phi_1 \sin(q_1+q_2).
\end{aligned}
$$

APPENDIX 2. NUMERICAL VALUES FOR SIMULATION

Parameter	Value	Unit
Young's modulus	$E_1 = E_2 = 1.06 \times 10^{11}$	N/m^2
Area moment of inertia	$I_1 = I_2 = 9.9 \times 10^{-12}$	m^4
Link length	$L_1 = L_2 = 1.05$	m
Link linear mass density	$\mu_1 = \mu_2 = 4.05 \times 10^{-1}$	kg/m
Actuator constants	$k_1 = 0.63$ and $k_2 = 0.18$	N-m and N-m/rad, respectively
Stall torque	$\tau_s = 0.63$	N-m
No-load speed	$w_0 = 3.5$	rad/sec
Initial joint angles	$q_1(0) = 0$ and $q_2(0) = 90$	degrees
Mass of end effector	$m_e = 0.1$	kg